# Three-Phase Distortion Analysis based on Space-Vector Locus Diagrams

DIEGO BELLAN
Department of Electronics, Information and Bioengineering,
Politecnico di Milano,
Piazza Leonardo da Vinci 32, 20133 Milan,
ITALY

*Abstract:* - This work deals with the use of the space vector concept to characterize the harmonic content of a three-phase voltage/current. It is shown that the shape of the trajectory of the space vector on the complex plane (i.e., the locus diagram) provides information about its harmonic content. In particular, it is shown that each harmonic contributes to the locus diagram with a number of lobes depending on the relative angular frequency between the harmonic and the fundamental component. To this aim, the different contributions of positive-sequence and negative-sequence harmonics is explained and put into evidence with specific examples. The expressions for the magnitude and phase of the space vector as functions of the harmonics are derived analytically. Numerical examples are provided to show how the locus diagram can represent a three-phase quantity with positive-sequence and negative-sequence harmonics.

*Key-Words:* - harmonic analysis, power quality, power system analysis, space vector, symmetrical component transformation, three-phase variables.

Received: April 11, 2023. Revised: October 26, 2023. Accepted: November 25, 2023. Published: December 31, 2023.

## 1 Introduction

Power quality is an issue of paramount importance in modern electrical systems. Many aspects, ranging from voltage/current magnitude and frequency variations, fluctuation, unbalance and harmonics have been extensively investigated in the relevant literature in the past decades, [1], [2], [3], [4], [5], [6], [7], [8], [9], [10], [11], [12]. One of the most interesting mathematical approaches for power quality assessment, emerged in recent years, is the use of the space vector concept in a three-phase system, [13], [14], [15], [16], [17], [18], [19], [20], [21], [22], [23]. A space vector is a time-domain complex-valued function representing a set of three phase variables (i.e., phase voltages or currents). Under ideal sinusoidal conditions the trajectory of the space vector on the complex plane (i.e., the locus diagram of the space vector) is a circle. In case of an event like a single-phase or a double-phase fault the locus diagram takes an elliptical shape. The geometrical characteristics of the space vector ellipse allow the detection and classification of the fault.

The use of the space-vector locus diagram for the distortion (i.e., harmonic) analysis of a three-phase system, however, is a new approach not yet exploited in the relevant literature. In fact, to the Author's knowledge, the idea of locus diagrams for harmonic analysis and power quality characterization can be found only in one paper in a very early stage, [24]. In that paper, the Authors propose the general idea that each harmonic can be identified by a specific shape of the locus diagram. However, that idea was not furtherly investigated, and no analytical details were provided.

In this work, the impact of harmonics on the locus diagram of a space vector is investigated analytically. In particular, by resorting to the series expansion of space vectors, the analytical expressions for the magnitude and the phase of the space vector are derived for each harmonic component. It is shown that the effect on the locus diagram is not related only to the harmonic order, but also to the positive or negative sequence of each harmonic, according to the well-known Symmetrical Component Transformation (SCT). Thus, the locus diagram of a space vector can provide information about the harmonic content in a very concise way. This is a unique property because, unlike a phasor diagram, a single locus diagram can fully represent a three-phase quantity with harmonics. From this viewpoint, the results derived in the paper provide an original contribution to power quality analysis of distorted three-phase variables.

The paper is organized as follows. In Section 2 the space vector definition and series expansion are

recalled. In Section 3 the expressions for the magnitude and phase of the space vector are analytically derived as functions of the harmonics of the three-phase quantity represented by the space vector. In Section 4 some numerical examples are shown in order to show typical shapes of locus diagrams for specific harmonics. Conclusions are presented in Section 5.

## 2 Space-Vector Series Expansion

Let us consider the time-domain phase currents $[i_a\ i_b\ i_c]^T$ at a specific point of a given three-phase system (the following derivations hold in the case where the phase voltages $[v_a\ v_b\ v_c]^T$ were considered instead of the currents).

The Clarke transformation of the phase currents $[i_a\ i_b\ i_c]^T$ is defined as, [25], [26]:

$$\begin{bmatrix} i_\alpha \\ i_\beta \\ i_0 \end{bmatrix} = \boldsymbol{T}\begin{bmatrix} i_a \\ i_b \\ i_c \end{bmatrix} = \sqrt{\frac{2}{3}}\begin{bmatrix} 1 & -\frac{1}{2} & -\frac{1}{2} \\ 0 & \frac{\sqrt{3}}{2} & -\frac{\sqrt{3}}{2} \\ \frac{1}{\sqrt{2}} & \frac{1}{\sqrt{2}} & \frac{1}{\sqrt{2}} \end{bmatrix}\begin{bmatrix} i_a \\ i_b \\ i_c \end{bmatrix} \quad (1)$$

where the transformation matrix $\boldsymbol{T}$ is orthogonal, i.e., $\boldsymbol{T}^{-1} = \boldsymbol{T}^T$, such that (1) is power invariant.

In the relevant literature it has been shown that under the assumption of a symmetrical three-phase system (i.e., a three-phase system consisting of components with equal phases and equal coupling between phases) the α and β variables defined through the Clarke transformation (1) fulfil the same equations. Thus, a new complex variable (i.e., the space vector) combining the α and β variables can be defined as:

$$\bar{\imath}(t) = i_\alpha(t) + j i_\beta(t) \quad (2)$$

where $j = \sqrt{-1}$. Therefore, the space vector is defined as a complex valued function whose real and imaginary parts are given by the α and β components, respectively, provided by the Clarke transformation (1).

Under sinusoidal steady-state conditions it can be shown that the space vector (2) can be written as:

$$\bar{\imath}(t) = I_p e^{j\omega t} + I_n^* e^{-j\omega t} \quad (3)$$

where asterisk denotes complex conjugate, whereas $I_p$ and $I_n$ are the positive- and negative-sequence phasor components, respectively, according to the well-known Symmetrical Component Transformation (SCT) in the phasor domain, [27], [28]:

$$\begin{bmatrix} I_p \\ I_n \\ I_0 \end{bmatrix} = \boldsymbol{S}\begin{bmatrix} I_a \\ I_b \\ I_c \end{bmatrix} = \frac{1}{\sqrt{3}}\begin{bmatrix} 1 & a & a^2 \\ 1 & a^2 & a \\ 1 & 1 & 1 \end{bmatrix}\begin{bmatrix} I_a \\ I_b \\ I_c \end{bmatrix} \quad (4)$$

where $a = e^{j2\pi/3}$.

Thus, under sinusoidal conditions, according to (3) the space vector (2) is given by the sum of two rotating phasors: the positive-sequence phasor $I_p$ rotating with positive angular frequency $+\omega$, and the complex conjugate of the negative-sequence phasor $I_n$ rotating with negative angular frequency $-\omega$. The corresponding trajectory of the space vector on the complex plane is elliptical, with semi-major and semi-minor axes given by $|I_p| + |I_n|$ and $\big||I_p| - |I_n|\big|$, respectively.

Under distorted conditions, i.e., periodic non-sinusoidal waveforms, the space vector (2) can be expanded in series, [23]. By adopting the well-known complex form of the Fourier series, we can write:

$$\bar{\imath}(t) = \sum_{k=-\infty}^{+\infty} I_k e^{jk\omega t} \quad (5)$$

where

$$I_k = \frac{1}{T}\int_0^T \bar{\imath}(t) e^{-jk\omega t} dt \quad (6)$$

Notice that, by generalizing (3), each frequency component $|k|\omega$ results in the sum of two components in the Fourier series (5), i.e.,

$$\bar{\imath}_k(t) = I_{|k|} e^{j|k|\omega t} + I_{-|k|} e^{-j|k|\omega t} \quad (7)$$

where the first component is the positive-sequence SCT component rotating with positive angular frequency $+|k|\omega$, whereas the second component is the negative-sequence (complex conjugate) SCT component rotating at negative angular frequency $-|k|\omega$.

Notice that, since the space vector is a complex valued function, the two Fourier coefficients $I_{|k|}$ and $I_{-|k|}$ are not related by complex conjugation, i.e., $I_{-|k|} \neq I_{|k|}^*$.

Thus, the Fourier series expansion (5) provides a double decomposition of the space vector. The first is the conventional frequency decomposition in harmonic frequencies $|k|\omega$. The second decomposition provides, for each harmonic component, the sequence decomposition in a positive sequence component rotating with positive angular frequency $+|k|\omega$, and a negative-sequence

component rotating with negative angular frequency $-|k|\omega$.

In the general case, all the frequency and sequence components can be found in the series expansion (5). In many applications, however, due to the phase symmetry of the three-phase system, the phase variables $i_a, i_b, i_c$ are characterized by the same distortion with $T/3$ time shift, i.e., $i_b(t) = i_a(t - T/3)$, and $i_c(t) = i_a(t + T/3)$. It means that the waveforms $i_b(t)$ and $i_c(t)$ are exact replicas of the distorted waveform $i_a(t)$ provided that a $T/3$ translation is introduced.

Under such assumption, with simple algebra it can be shown that the series expansion (5) can include only the frequency components with frequency index $k = 1 + 3m$ with $m = 0, \pm1, \pm2, \pm3, ...$, [29], [30]. Thus, according to the double decomposition outlined above, the allowed positive-sequence harmonics are given by the list $\{I_1, I_4, I_7, I_{10}, \dots\}$, whereas the allowed negative-sequence harmonics are given by $\{I_{-2}, I_{-5}, I_{-8}, I_{-11}, \dots\}$.

## 3 Space-Vector Locus Diagrams

The space vector defined in (2) is a complex valued function of time whose trajectory on the complex plane, according to (5), can provide information about the harmonic content and the sequence decomposition. In this Section the main properties of such trajectories, called locus diagrams, will be investigated under the assumption of symmetrical phase distortion introduced at the end of Section II.

The simplest case is the sinusoidal non-distorted case (see (3)). Indeed, when only the fundamental component $I_1$ is present it means that only the positive-sequence component $I_p = I_1$ at fundamental frequency is present. The corresponding locus diagram of the space vector rotating with positive angular frequency $+\omega$ is a circle with radius $|I_1|$.

According to the assumption of symmetrical phase distortion, the next harmonic component is $I_{-2}$, i.e., a negative-sequence (complex conjugate) phasor rotating with negative angular frequency $-2\omega$. The resulting space vector is the sum of the two rotating phasors. Notice that, in terms of relative rotation, the second harmonic phasor is rotating with angular frequency $-3\omega$ with respect to the fundamental frequency phasor. The two rotating phasors and the resulting space vector are depicted in Figure 1. For the sake of simplicity, we assumed that the two phasors were aligned at $t = 0$. By using the well-known cosine rule the magnitude of the space vector can be readily evaluated:

$$|\bar{\imath}(t)| = \sqrt{|I_1|^2 + |I_{-2}|^2 - 2|I_1||I_{-2}|\cos(\pi - 3\omega t)}$$

$$= \sqrt{|I_1|^2 + |I_{-2}|^2 + 2|I_1||I_{-2}|\cos(3\omega t)} \quad (8)$$

By introducing normalization with respect to the fundamental component $|I_1|$ we obtain:

$$i(t) = \frac{|\bar{\imath}(t)|}{|I_1|} = \sqrt{1 + r_2^2 + 2r_2\cos(3\omega t)} \quad (9)$$

where $r_2 = |I_{-2}|/|I_1|$. Notice the term $3\omega t$ in (9) due to the relative angular frequency between the rotating phasors $I_1$ and $I_{-2}$. Indeed, as far as the next harmonic is considered, i.e., the rotating positive-sequence phasor $I_4$, from Figure 2 and by using the cosine rule we obtain a n expression similar to (9):

$$i(t) = \frac{|\bar{\imath}(t)|}{|I_1|} = \sqrt{1 + r_4^2 + 2r_4\cos(3\omega t)} \quad (10)$$

where $r_4 = |I_4|/|I_1|$.

The above results can be generalized to the contribution of any harmonic. Indeed, by considering that the allowed harmonic indices are given by $k = 1 + 3m$, the corresponding normalized absolute value of the space vector is given by:

$$i(t) = \frac{|\bar{\imath}(t)|}{|I_1|} = \sqrt{1 + r_k^2 + 2r_k\cos(3m\omega t)} \quad (11)$$

Notice that since $m = 0, \pm1, \pm2, \pm3, ...$, the same behavior is obtained for each positive and negative value of $m$, i.e., for two rotating phasors (one positive-sequence and one negative-sequence phasor). Thus, the two phasors $I_4$ and $I_{-2}$ ($m = \pm1$) rotating at the same relative angular frequency $3\omega$ with respect to $I_1$, the two phasors $I_7$ and $I_{-5}$ ($m = \pm2$) rotating at the same relative angular frequency $6\omega$ with respect to $I_1$, and so on.

Although the time behavior of the space vector magnitude (9) and (10) is the same, from Figure 1 and Figure 2 it is apparent that the space vector phase $\varphi(t)$ is different in the two cases.
From Figure 1, by using the sine rule:

$$\frac{|\bar{\imath}(t)|}{\sin(\pi - 3\omega t)} = \frac{|I_{-2}|}{\sin(\omega t - \varphi(t))} \quad (12)$$

we obtain:

$$\varphi(t) = \omega t - \arcsin\left(\frac{r_2}{i(t)}\sin(3\omega t)\right) \quad (13)$$

where $i(t)$ is given by (9).

Similarly, for the case in Figure 2 we obtain:

$$\varphi(t) = \omega t + \arcsin\left(\frac{r_4}{i(t)}\sin(3\omega t)\right) \quad (14)$$

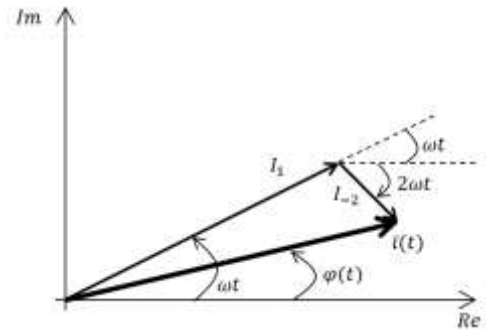


Fig. 1: Rotating phasors and space vector in the case of a negative-sequence second harmonic

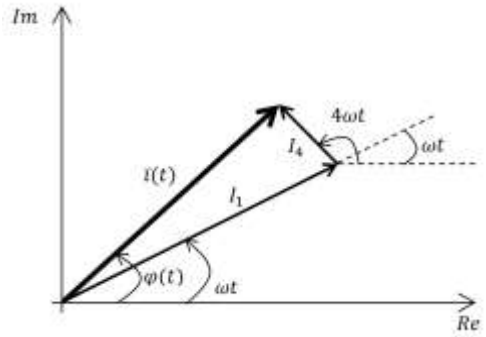


Fig. 2: Rotating phasors and space vector in the case of a positive-sequence fourth harmonic

where $i(t)$ is given by (10).

Notice the negative sign in (13) related to the phasor $I_{-2}$ rotating with negative angular frequency, whereas the positive sign in (14) related to the phasor $I_4$ rotating with positive angular frequency.

Thus, in the general case we can write:

$$\varphi(t) = \omega t + \arcsin\left(\frac{r_k}{i(t)}\sin(m\omega t)\right) \quad (15)$$

where $m = 0, \pm1, \pm2, \pm3, \ldots$ provides the right sign in the equation.

Finally, the space-vector locus diagram is the diagram of the complex valued function with magnitude $i(t)$ and phase $\varphi(t)$.

# 4 Numerical Validation and Investigation

In this Section, (11) and (15) are used to draw locus diagrams of space vectors under distorted conditions. Typical shapes of locus diagrams will be obtained and discussed.

As a first example, let us consider the following phase currents including fundamental and second harmonic components: $i_a(t) = \sqrt{2}[1 \cdot \cos(\omega t) + 0.3 \cdot \cos(2\omega t)]$, $i_b(t) = i_a(t - T/3)$, $i_c(t) = i_a(t + T/3)$. Notice the large relative magnitude of the second harmonic (i.e., 30%) to the aim of highlighting its effects on the locus diagram. By using (9) and (13) (i.e., the general results (11) and (15) specialized to the second harmonic) the locus diagram represented by the black line in Figure 3 was obtained. Notice the three lobes due to the relative angular frequency $3\omega$ between the fundamental and the negative-sequence second harmonic. Moreover, notice the sharp shape of the three lobes due to the fact that the two rotating phasors (Figure 1) rotate in the opposite direction. The blue line in Figure 3 shows the case of the fourth harmonic, i.e., $i_a(t) = \sqrt{2}[1 \cdot \cos(\omega t) + 0.3 \cdot \cos(4\omega t)]$, $i_b(t) = i_a(t - T/3)$, $i_c(t) = i_a(t + T/3)$. Also in this case we obtain three lobes because the relative angular frequency between the fundamental and the fourth harmonic is still $3\omega$. However, notice that the shape of the lobes in this case is round, due to the fact that the two rotating phasors rotate in the same direction (Figure 2). The red line in Figure 3 shows the case where both the second and the fourth harmonics are present with equal magnitude, i.e., $i_a(t) = \sqrt{2}[1 \cdot \cos(\omega t) + 0.15 \cdot \cos(2\omega t) + 0.15 \cdot \cos(4\omega t)]$, $i_b(t) = i_a(t - T/3)$, $i_c(t) = i_a(t + T/3)$. The resulting locus diagram has an intermediate behavior between the black and the blue lines.

The second example, represented in Figure 4, is related to the case of fifth and seventh harmonics. In particular, the black line in Figure 4 corresponds to the case of fifth harmonic, i.e., it was assumed $i_a(t) = \sqrt{2}[1 \cdot \cos(\omega t) + 0.2 \cdot \cos(5\omega t)]$, $i_b(t) = i_a(t - T/3)$, $i_c(t) = i_a(t + T/3)$. Notice that, since in this case the relative angular frequency between the fundamental and the negative-sequence fifth harmonic is $6\omega$, the number of lobes is six. Also in this case the sharp shape of the lobes can be observed due to the fact that the two rotating phasors rotate in the opposite direction. On the contrary, when the seventh harmonic is considered (blue line), i.e., $i_a(t) = \sqrt{2}[1 \cdot \cos(\omega t) + 0.2 \cdot \cos(7\omega t)]$, $i_b(t) = i_a(t - T/3)$, $i_c(t) =$

$i_a(t+T/3)$, the six lobes have round shape because the two rotating phasors rotate in the same direction. When both the fifth and the seventh harmonics are present, i.e., $i_a(t) = \sqrt{2}[1 \cdot \cos(\omega t) + 0.1 \cdot \cos(5\omega t) + 0.1\cos(7\omega t)]$, $i_b(t) = i_a(t-T/3)$, $i_c(t) = i_a(t+T/3)$, the corresponding behavior (red line) is intermediate between the black and the blue lines.

Figure 5 shows the case of fifth and seventh harmonics with phases different from zero. In this specific case, the phase of the fundamental was assumed $\pi/6$, whereas for the fifth and the seventh harmonics the phases were assumed $\pi/4$ and $\pi/3$, respectively. Notice that the locus diagrams show same shapes and a simple rotation with respect to Figure 4 due to the phases different from zero.

Figure 6 shows an example of mixed harmonics, i.e., rotating phasors with different relative angular frequency with respect to the fundamental. In this case it was assumed $i_a(t) = \sqrt{2}[1 \cdot \cos(\omega t) + 0.3 \cdot \cos(2\omega t) + 0.2 \cdot \cos(5\omega t)]$, $i_b(t) = i_a(t-T/3)$, $i_c(t) = i_a(t+T/3)$. The second harmonic is responsible of three lobes as in Figure 3, whereas the fifth harmonic is responsible of six lobes as in Figure 4. Notice that the characteristic marks of both the harmonics can be still observed in Figure 6. Of course, in the more general case where many harmonics are present, it is expected that the characteristic shape of each harmonic cannot be clearly identified. Thus, the analysis derived in this work is mainly devoted to the case where the frequency spectrum has one dominant harmonic.

## 5 Conclusion

The locus diagram of a space vector has been used to provide a concise representation of a three-phase variable with harmonics. It has been shown that the number of lobes of the diagram is related to the harmonic order, whereas the shape of the lobes is related to the positive or negative sequence of the harmonic. In fact, the number of lobes depends on the relative angular frequency between the harmonic and the fundamental components. Thus, for example, it was made clear that a positive-sequence fourth harmonic provides the same number of lobes (i.e., three) as a negative-sequence second harmonic because both space vectors rotate with angular frequency equal to three times the angular frequency of the fundamental component. Similar considerations can be extended to higher order harmonics.

Future work will be devoted to further investigate the analytical properties of locus diagrams, with particular focus on the case of superposition of harmonics with similar magnitude. Indeed, the results proposed in this paper hold in the case of one dominant harmonic. However, in many practical cases the concurrent contribution of several significant harmonics must be evaluated.

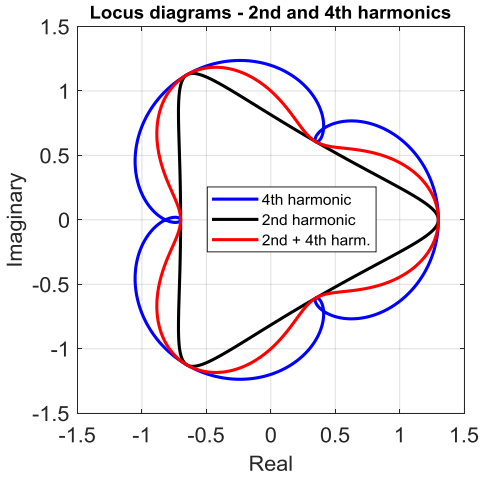


Fig. 3: Locus diagram of the space vector in case of second harmonic (black line), fourth harmonic (blue line), and both the harmonics (red line)

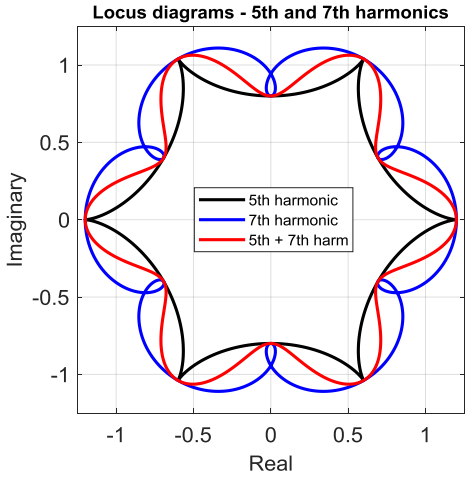


Fig. 4: Locus diagram of the space vector in case of fifth harmonic (black line), seventh harmonic (blue line), and both the harmonics (red line)

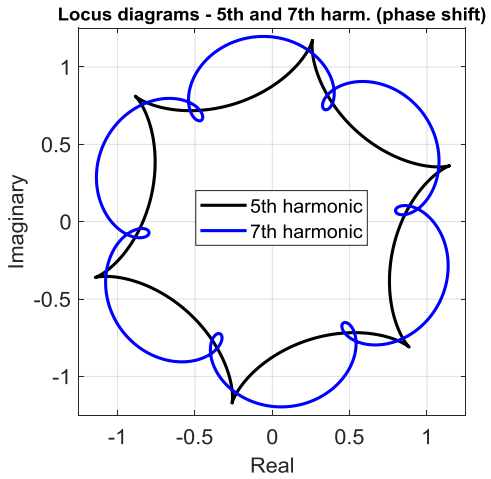


Fig. 5: Locus diagram of the space vector in case of fifth harmonic (black line) and seventh harmonic (blue line) with phases different from zero. A change in the phase values results in diagram rotation with respect to Figure 4

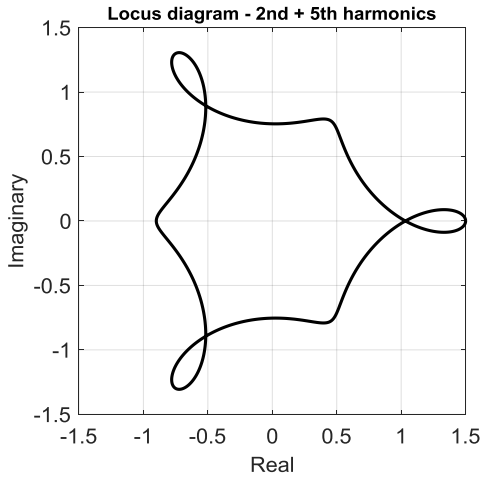


Fig. 6: Locus diagram of the space vector in case of both second and fifth harmonics. The three lobes corresponding to the second harmonic (Figure 3) and the six lobes corresponding to the fifth harmonic (Figure 4) can be still observed

*References:*

[1] R. C. Dugan, S. Santoso,M. F.McGranaghan, and H.Wayne Beaty, *Electrical Power Systems Quality*, vol. 2. New York, NY, USA: Mcgraw-Hill, 1996.

[2] M. H. Bollen, *Understanding Power Quality Problems: Voltage Sags and Interruptions*. New York, NY, USA: Wiley-IEEE, 2000.

[3] *IEEE Recommended Practice for Monitoring Electric Power Quality*, IEEE Std 1159-2009 (Revision of IEEE Std 1159-1995), Jun. 2009.

[4] P. Wei, Y. Xu, Y. Wu, and C. Li, "Research on the classification of voltage sag sources based on recorded events," *CIRED-Open Access Proc. J.*, vol. 2017, no. 1, pp. 846-850, 2017.

[5] H. Liao, J. V. Milanovic, M. Rodrigues, and A. Shenfield, "Voltage sag estimation in sparsely monitored power systems based on deep learning and system area mapping," *IEEE Trans. Power Del.*, vol. 33, no. 6, pp. 3162-3172, Dec. 2018.

[6] E. Styvaktakis, M. H. J. Bollen, and I. Y. H. Gu, "Expert system for classification and analysis of power system events," *IEEE Trans. Power Del.*, vol. 17, no. 2, pp. 423-428, Apr. 2002.

[7] C. Venkatesh, D. V. S. S. Siva Sarma, and M. Sydulu, "Classification of voltage sag, swell, and harmonics using S-transform based modular neural network," in *Proc. 14th Int. Conf. on Harmonics and Quality of Power*, Bergamo, Italy, 2010, pp. 1-7.

[8] K. M. Silva, B. A. Souza, and N. S. D. Brito, "Fault detection and classification in transmission lines based on wavelet transform and ANN," *IEEE Trans. Power Del.*, vol. 21, no. 4, pp. 2058-2063, Oct. 2006.

[9] P. Janik and T. Lobos, "Automated classification of power-quality disturbances using SVM and RBF networks," *IEEE Trans. Power Del.*, vol. 21, no. 3, pp. 1663-1669, Jul. 2006.

[10] M. Manjula, A.V. R. S. Sarma, and S. Mishra, "Detection and classification of voltage sag causes based on empirical mode decomposition," in *Proc. 2011 Annual IEEE India Conf.*, Hyderabad, India, 2011, pp. 1-5.

[11] Aboyede Abayomi, Agha F. Nnachi, "Analysis of Distribution Static Compensator Control Strategies for Mitigating Voltage Dip Impact on Distribution Network," *WSEAS Transactions on Power Systems*, vol. 18, pp. 301-309, 2023, https://doi.org/10.37394/232016.2023.18.31.

[12] Tseligorov N. A., Ozersky A. I., Chubukin A. V., Tseligorova E. N., "Development of a Robust Scalar Control System for an Induction Squirrel-cage Motor Based on a Linearized Vector Model," *WSEAS Transactions on Computers*, vol. 21, pp. 1-9, 2022, https://doi.org/10.37394/23205.2022.21.1.

[13] V. Ignatova, P. Granjon, and S. Bacha, "Space vector method for voltage dips and swells analysis," *IEEE Trans. on Power Delivery*, vol. 24, no. 4, pp. 2054-2061, 2009.

[14] M. R. Alam, K. M. Muttaqi, and A. Bouzerdoum, "Characterizing voltage sags and swells using three-phase voltage ellipse parameters," *IEEE Trans. Ind. Appl.*, vol. 51, no. 4, pp. 2780–2790, Jul. 2015.

[15] J. R. Camarillo-Peñaranda and G. Ramos, "Fault classification and voltage sag parameter computation using voltage ellipses," *IEEE Trans. Ind. Appl.*, vol. 55, no. 1, pp. 92–97, Jan./Feb. 2019.

[16] J. R. Camarillo-Peñaranda and G. Ramos, "Characterization of voltage sags due to faults in radial systems using three-phase voltage ellipse parameters," *IEEE Trans. Ind. Appl.*, vol. 54, no. 3, pp. 2032–2040, May/Jun. 2018.

[17] T. García-Sánchez, E. Gómez-Lázaro, E. Muljadi, M. Kessler, A. Molina-García, "Approach to fitting parameters and clustering for characterising measured voltage dips based on two-dimensional polarisation ellipses," *Renewable Power Generation IET*, vol. 11, no. 10, pp. 1335-1343, 2017.

[18] A. Bagheri, M. J. H. Bollen, "Space phasor model based monitoring of voltages in three phase systems", *18th International Conference on Harmonics and Quality of Power (ICHQP)*, 2018, pp. 1-6.

[19] S. Li, L. Xie and Y. Liu, "Fast Identification Method for Voltage Sag Type and Characteristic," *IECON 2019 - 45th Annual Conference of the IEEE Industrial Electronics Society*, Lisbon, Portugal, 2019.

[20] A. Bagheri, M. H. J. Bollen, I. Y. H. Gu, "Improved characterization of multi-stage voltage dips based on the space phasor model", *Electric Power Systems Research*, vol. 154, pp. 319, 2018.

[21] M. R. Alam, K. M. Muttaqi, and A. Bouzerdoum, "A new approach for classification and characterization of voltage dips and swells using 3-D polarization ellipse parameters," *IEEE Trans. Power Delivery*, vol. 30, no. 3, pp. 1344–1353, Jun. 2015.

[22] M. R. Alam, K. M. Muttaqi and T. K. Saha, "Classification and Localization of Fault-Initiated Voltage Sags Using 3-D Polarization Ellipse Parameters," *IEEE Transactions on Power Delivery*, vol. 35, no. 4, pp. 1812-1822, Aug. 2020.

[23] D. Bellan, "Probability Density Function of Three-Phase Ellipse Parameters for the Characterization of Noisy Voltage Sags," *IEEE Access*, vol. 8, pp. 185503-185513, 2020.

[24] C. J. O'Rourke, M. M. Qasim, M. R. Overlin, J. L. Kirtley, "A Geometric Interpretation of Reference Frames and Transformations: dq0, Clarke and Park," *IEEE Trans. on Energy Conversion*, vol. 34, pp. 2070-2083, 2019.

[25] D. Bellan, "Analytical Investigation of the Properties of Transients in Unbalanced Three-Phase Four-Wire Networks," *Energies*, vol. 15, pp. 1-26, 2022.

[26] D. Bellan, "Clarke transformation solution of asymmetrical transients in three-phase circuits," *Energies*, vol. 13, pp. 1-19, 2020.

[27] J. C. Das, *Understanding Symmetrical Components for Power System Modeling*, NJ, USA: Wiley, 2017.

[28] G. Chicco, A. Mazza, "100 Years of Symmetrical Components," *Energies*, vol. 12, pp. 1-20, 2019.

[29] G. Superti-Furga, S. Barcellona and E. Tironi, "Space-vector approach in three-phase unbalance and distortion analysis," *17th International Conference on Harmonics and Quality of Power (ICHQP),* Belo Horizonte, Brazil, 2016, pp. 721-726.

[30] S. Barcellona, S. Negri and G. Superti-Furga, "Space-vector analysis of harmonic distortion in three-phase PWM," *18th International Conference on Harmonics and Quality of Power (ICHQP),* Ljubljana, Slovenia, 2018, pp. 1-6.

**Contribution of Individual Authors to the Creation of a Scientific Article (Ghostwriting Policy)**

The authors equally contributed in the present research, at all stages from the formulation of the problem to the final findings and solution.

**Sources of Funding for Research Presented in a Scientific Article or Scientific Article Itself**

No funding was received for conducting this study.

**Conflict of Interest**

The authors have no conflicts of interest to declare.